Cell Reports
Article

Aging Yeast Cells Undergo a Sharp Entry into Senescence Unrelated to the Loss of Mitochondrial Membrane Potential

Steffen Fehrmann,[1] Camille Paoletti,[1] Youlian Goulev,[1] Andrei Ungureanu,[3] Hugo Aguilaniu,[2] and Gilles Charvin[1,*]
[1]Institut de Génétique et de Biologie Moléculaire et Cellulaire, 1 Rue Laurent Fries, 67400 Illkirch Cedex, France
[2]LBMC, ENS Lyon, 46 Allée d'Italie, 69364 Lyon Cedex 07, France
[3]LJC, ENS Lyon, 46 Allée d'Italie, 69364 Lyon Cedex 07, France
*Correspondence: charvin@igbmc.fr
http://dx.doi.org/10.1016/j.celrep.2013.11.013

SUMMARY

In budding yeast, a mother cell can produce a finite number of daughter cells before it stops dividing and dies. Such entry into senescence is thought to result from a progressive decline in physiological function, including a loss of mitochondrial membrane potential ($\Delta\Psi$). Here, we developed a microfluidic device to monitor the dynamics of cell division and $\Delta\Psi$ in real time at single-cell resolution. We show that cells do not enter senescence gradually but rather undergo an abrupt transition to a slowly dividing state. Moreover, we demonstrate that the decline in $\Delta\Psi$, which is observed only in a fraction of cells, is not responsible for entry into senescence. Rather, the loss of $\Delta\Psi$ is an age-independent and heritable process that leads to clonal senescence and is therefore incompatible with daughter cell rejuvenation. These results emphasize the importance of quantitative single-cell measurements to decipher the causes of cellular aging.

INTRODUCTION

Budding yeast cells divide asymmetrically, with each mother cell producing a limited number (~25) of smaller daughter cells before it enters senescence and eventually dies (Mortimer and Johnston, 1959). Remarkably, daughters of aged mother cells recover a full replicative lifespan (RLS; total number of cell divisions), which implies that a rejuvenation mechanism exists to avert clonal senescence (Kennedy et al., 1994). Although a large number of mutations are known to modulate RLS, the precise causes of senescence and rejuvenation, and thus their heritability, are poorly understood.

Several theories of replicative senescence based on the retention of potentially deleterious cellular components by mother cells have been proposed. Aging mothers accumulate extrachromosomal ribosomal DNA circles (ERCs) in their nucleoli, which are thought to interfere with the regulation of gene expression (Sinclair and Guarente, 1997). However, the mechanism by which ERCs are asymmetrically segregated is still under debate (Shcheprova et al., 2008; Gehlen et al., 2011; Khmelinskii et al., 2011), and it is not clear how ERCs are toxic to mother cells. Carbonylated proteins have also been shown to accumulate in aging cells and form aggregates that are asymmetrically inherited by the mother cells upon division (Aguilaniu et al., 2003; Erjavec et al., 2007), but direct evidence that carbonylated proteins cause replicative senescence is still missing. In addition, the putative mechanism of aggregates retention by mothers is still controversial (Zhou et al., 2011; Spokoini et al., 2012; Liu et al., 2010).

A third model proposes that aging is tightly associated with mitochondrial dysfunction in yeast (Guarente, 2008) and in higher eukaryotes (Wallace, 2005; Houtkooper et al., 2013). Various events have been linked to the age-dependent loss of mitochondrial function, including changes in the maintenance of mtDNA integrity, mitochondrial dynamics and recycling, and the production of reactive oxygen species (Seo et al., 2010). In yeast, for instance, it was shown that a reduction in mitochondrial fission increases longevity (Scheckhuber et al., 2007). Recent studies also showed that damaged oxidized mitochondria are preferentially retained by mother cells, suggesting a role for these organelles in daughter cell rejuvenation (McFaline-Figueroa et al., 2011).

A decline in mitochondrial membrane potential ($\Delta\Psi$), which is required for respiration competence, has also been associated with age-dependent mitochondrial dysfunction (Lai et al., 2002). More recently, Veatch et al. (2009) showed that the vast majority of old mother cells generate *petite* daughters, which are slow-growing cells with a respiration defect due to mutations or the complete loss of mtDNA. The authors suggested that an age-dependent loss in $\Delta\Psi$ in mothers leads to a progressive decline in growth rate and ultimately triggers genomic instability via a defect in the biogenesis of iron-sulfur-cluster-containing proteins, which may be directly involved in genome maintenance (Veatch et al., 2009). Further work proposed that the loss of $\Delta\Psi$ results from an early (up to the fourth cell division) loss of vacuolar acidity (Hughes and Gottschling, 2012), which hampers pH-dependent transport of neutral amino acids and disrupts $\Delta\Psi$

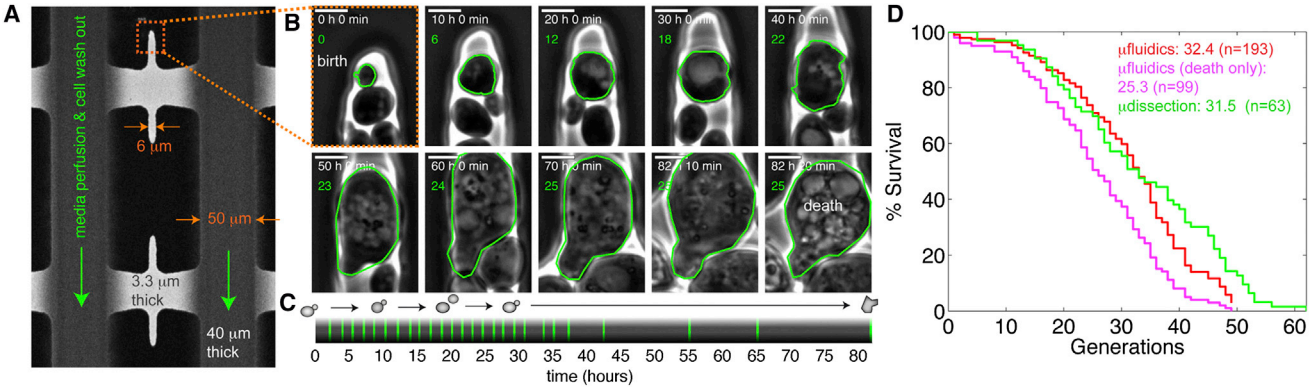

Figure 1. Principle of the Microfluidic Device and Tracking of Mother Cells

(A) Image of the CLiC microfluidic device.

(B) Sequence of phase contrast images taken at the indicated time points over the cell lifespan. The green contours highlight the cell of interest, and the green numbers indicate the replicative age. The scale bar represents 4 μm.

(C) Graphical representation of the lifespan of the cell shown in (B). The green vertical lines indicate the times at which budding occurred.

(D) Survival probability curves of cells growing in the microfluidic device (Kaplan-Meier estimator with [red curve] or without [magenta curve] censored events) or cells analyzed in a standard microdissection experiment (green curve).

See also Figures S1–S4 and Movie S1.

by an unknown mechanism. Interestingly, vacuole acidity is restored in young daughter cells (Hughes and Gottschling, 2012), providing an attractive potential connection between loss of $\Delta\Psi$, entry into senescence, and daughter rejuvenation.

One of the major barriers to understanding the mechanisms that drive cells into senescence is the difficulty in tracking the fate of single aging cells in real time. For instance, the most common method of measuring RLS, physical microdissection of cells, provides no information on cell physiology and is not suitable for monitoring molecular markers in aging cells. Cell sorting (Kennedy et al., 1994; Aguilaniu et al., 2003; Unal et al., 2011) and "mother enrichment" techniques (Lindstrom and Gottschling, 2009; Afonso et al., 2010) have been used successfully to examine the physiology of aging cells (Hughes and Gottschling, 2012). However, these techniques provide static snapshots of a cell population that may mask the complex dynamic behavior of individual cells. Very recently, several biophysical strategies have been developed that reveal the potential of microfluidics technology for aging studies in bacteria (Wang et al., 2010) and yeast (Lee et al., 2012; Xie et al., 2012; Zhang et al., 2012).

Here, we report the development of a microfluidic device and quantitative image analysis platform that allows microscopic monitoring of successive divisions of single cells over their entire lifespan with high temporal resolution. Combining this technique with a computational approach, we revisit and challenge two important concepts established in recent yeast-aging studies. First, in contrast to the notion that cells undergo a progressive decline in proliferation, we show that cellular senescence follows a very abrupt transition to a slow growth regime, which we named the senescence entry point (SEP). Second, we demonstrate that the SEP is unrelated to a loss of $\Delta\Psi$ and/or to the formation of *petite* cells. Indeed, we show that the decline in $\Delta\Psi$ observed in some cells is an age-independent process that leads to clonal senescence and is thus incompatible with daughter cell rejuvenation. Finally, we report a phenomenon of cell-cycle-dependent oscillations in mitochondrial fusion and fission that may play a role in the mother/daughter segregation of mitochondria, as suggested by a previous study (McFaline-Figueroa et al., 2011).

RESULTS

A Device for Tracking Cell Fate from Birth to Death

One of the limitations inherent to classical aging studies in yeast is the inability to track cells in real time over their lifespan. To overcome this, we developed a custom microfluidic device that allows microscopic visualization of successive divisions of single yeast cells from birth to death. The device was designed to monitor a single mother *c*ell *l*oaded *i*nto a *c*avity and is therefore termed CLiC. Cells in exponential growth phase are loaded into an array of "trapping areas" (length × width × height, 90 × 40 × 3.3 μm; Figures 1A and S1A) and allowed to proliferate for the duration of the experiment (typically 120 hr). The trapping areas are connected to supply channels that ensure continuous media replenishment and allow excess cells to be flushed out of the device.

Cell proliferation within the trapping area leads to colonization of the small cavities (6 μm wide) by a few cells (Figure S1B). Due to the axial budding pattern of haploid cells, a cell that reaches the enclosed tip of the cavity (referred to as a CLiC cell) tends to bud toward the cavity exit (Figures S1C and S1D), allowing successive divisions to be monitored over time (Figure 1B and Movie S1). However, it is possible that the CLiC cell could eventually leave the cavity due to occasional polarity switches and random cell rotation. Despite this limitation, we found the probability of losing a cell during its lifespan was <35%, which outperforms a previous microfluidic device that reported 50% cell loss within the first 10 hr and more than 70% in total (Lee et al., 2012). Up to 60 cavities in the CLiC device can be imaged (phase contrast and fluorescence) in parallel during the

time-lapse interval of 10 min. Thus, by monitoring the budding events of individual CLiC cells, we are able to follow the dynamics of division (Figure 1C) and determine the RLS of each cell.

Using this methodology, we observed a reproducible median RLS of 32.4 ± 1.4 generations for the BY4741 strain in synthetic complete dextrose (SCD) medium (based on Kaplan-Meier estimator; n = 191 cells; Figure 1D). This value was not significantly different (log rank test; p = 0.3) from the RLS obtained using a standard microdissection technique (31.5 ± 1; n = 63; Figure 1D) but was slightly higher than RLS values reported for earlier versions of microfluidic devices (21 divisions in SCD [Lee et al., 2012] and <20 in yeast extract peptone dextrose [YPD] [Xie et al., 2012]). The Kaplan-Meier estimator used to measure the RLS allows one to take into account cells that leave the trapping area before death (such events are known as "right-censored" in standard survival analysis). Therefore, this method provides an unbiased estimation of the mean RLS in the microfluidics device, which can be compared to microdissection experiments. For the remainder of the study, however, only cells dying within the trapping area were included in the analyses, for which the median RLS was 25.3 ± 1 (n = 125; Figure 1D).

Although the similarity of the results obtained with the microdissection and microfluidics methodologies suggested that the CLiC device did not affect cell survival, CLiC cells at the tip of the cavity are relatively confined. Therefore, we measured the kinetics of medium diffusion/convection through a trapping area fully loaded with cells and verified that the medium flow was indeed sufficient to ensure adequate nutrient supply to the cavity tips (Figure S2; Supplemental Information). In addition, the mean division time of young mother cells in the CLiC device (Tdiv = 78.3 ± 0.5 min) was similar to that in other microfluidic devices (Charvin et al., 2008).

The Senescence Entry Point Marks the Sharp Transition to a Slowly Replicating State

Early studies used standard microdissection techniques to investigate the RLS of individual yeast cells (Egilmez and Jazwinski, 1989; Kennedy et al., 1994; Bitterman et al., 2003) and showed that the average division time increased with generation number. This key observation suggested that mother cells undergo a progressive age-associated decline in cellular function and eventually reach a state of replicative senescence.

To investigate the dynamics of cell division in aging yeast cells, we measured the division times of individual CLiC cells (using custom MATLAB software phyloCell; Supplemental Information). Analysis of division frequency as a function of generation number unexpectedly revealed that most cells underwent a sharp transition from a fast to a rapidly declining division rate (Figure 2A). We developed a routine to analyze the dynamics of division of individual cells and align all the traces to the point of entry into the slow division mode, which allowed us to separate the lifespan into healthy and senescent phases and to cluster the data according to the number of generations after entry into senescence (Figure 2B). When the division times of the aligned trajectories were averaged, we calculated that the cells transitioned from Tdiv = 78.3 ± 0.5 min (n = 1,172) to Tdiv = 238 ± 11 min (n = 188) in less than three divisions (Figures 2C and S3). We termed this abrupt transition the senescence entry point, or SEP.

These results are in striking contrast to the classical view that cellular aging is associated with a gradual decrease in replicative potential. The switch-like transition would not have been detected in studies in which division times were quantified by averaging the cell trajectories from birth (Kennedy et al., 1994), which results in pooling of the division events of short- and long-lived cells (Figures S4A and S4B). Recent work attempted to eliminate this artifact by synchronizing cell trajectories from death (Lee et al., 2012; Xie et al., 2012; Figures S4C and S4D). However, when we synchronized our data from birth, death, and SEP (Figure S4), the coefficients of variation (CV) of the division timings indicated that our in silico synchronization procedure more successfully limited intersample variability and therefore provided a more appropriate way to group the individual trajectories (see Figures S4E and F). Last, we also observed an abrupt transition to senescence using the microdissection assay, in which dissection timing records allowed us to estimate cell-cycle durations (see Figures S4G and S4H).

Strikingly, the two distinct physiological phases followed different statistics. Before the SEP, cells underwent an average of 19.2 ± 1.0 generations (CV = 0.42) according to a roughly Gaussian distribution (Figure 2D); in contrast, the number of generations in the post-SEP senescent state (mean 5.4 ± 0.6 generations; CV = 0.92) was exponentially distributed (Figure 2E). The number of cell divisions in the healthy and senescent phases of the lifespan did not correlate (correlation coefficient <0.1; data not shown), emphasizing the clear demarcation of the physiological states. Finally, the large increase in the CV of division times before and after the SEP (<0.2 and >0.6, respectively; Figure 2C) suggests that loss of control of the cell cycle is an important hallmark of the onset of senescence.

The SEP Is Not Linked to a Decline in $\Delta\Psi$

Veatch et al. (2009) recently proposed that aging mother cells, which eventually produce *petite* daughters, undergo a mitochondrial crisis leading to growth defects and increased genomic instability. This model was further supported by direct evidence that aging mothers experience a decline in mitochondrial membrane potential (Hughes and Gottschling, 2012). We therefore reasoned that the SEP and consequent growth slowdown observed here should fit this model of senescence-associated mitochondrial dysfunction.

To test this, we used a strain carrying two fluorescent mitochondrial markers, Tom70-GFP (green) and preCox4-mCherry (red), developed by Veatch et al. (2009), for real-time monitoring of the onset of mitochondrial dysfunction in aging mothers. Tom70 is a component of the nuclear-encoded protein import complex located at the outer mitochondrial membrane and thus serves as a mitochondrial marker, whereas preCox4 is the inner mitochondrial membrane targeting presequence of Cox4. Cox4 is a protein that requires $\Delta\Psi$ for mitochondrial import. It was shown previously that the decrease in preCox4-mCherry mitochondrial localization coincides with a decline in the $\Delta\Psi$–dependent $DiOC_6$ mitochondrial staining in ethidium-bromide-treated cells (Veatch et al., 2009) as well as in aging cells (Hughes and Gottschling, 2012). We confirmed that the

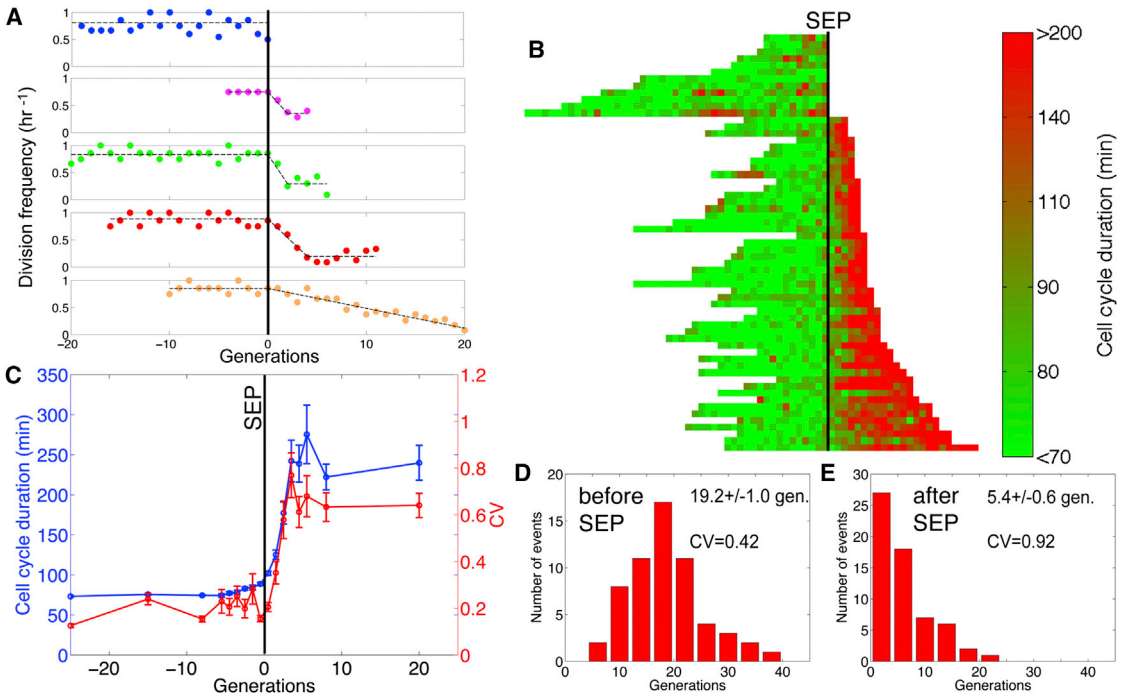

Figure 2. Yeast Cells Undergo a Sharp Transition to Senescence

(A) Frequency of cell division as a function of generation number for four representative cells (colored points). The black dashed line is the best fit to a piecewise function that assumes a constant division rate before senescence, a decay regime upon entry into senescence, and a constant division rate in the senescent state. All traces are synchronized to the senescence entry point (SEP).

(B) Clustered display of cell division trajectories resulting from the synchronization based on division frequency (as described in [A]). Each horizontal line (n = 61) represents a single mother cell, and each segment corresponds to one cell division. The lines are clustered vertically according to the duration of post-SEP survival from short (top) to long (bottom). Color coding represents cell-cycle duration.

(C) Mean cell-cycle duration (blue curve) and CV (red curve) for the data shown in (B).

(D and E) Distribution of number of generations undergone by mother cells before (D) and after (E) the SEP (n = 61).

level of preCox4-mCherry mitochondrial fluorescence was tightly correlated to the $DiOC_6$ signal in a population of exponentially growing cells (Figure S5). Therefore, this fluorescent marker serves as a relevant proxy for $\Delta\Psi$. We used our custom software phyloCell to delineate the contours of mitochondrial structures using the Tom70-GFP signal (Figures 3A and 3B) and then quantified the mean mitochondrial fluorescence levels of Tom70-GFP and preCox4-mCherry in individual cells (Figures 3C and 3D).

Strikingly, we observed that, in some cells, the preCox4-mCherry fluorescence within the mitochondria eventually vanished (Figures 3A and 3C) but in other cells was maintained at consistently high levels throughout their lifespan (Figures 3B and 3D; see also Figure S6 and Movie S3). The loss of mitochondrial preCox4-mCherry fluorescence was consistent with experiments in which cells were treated with ethidium bromide to induce mtDNA mutation (Figure S7), as described previously (Veatch et al., 2009). We used a piecewise linear model (Figure 3C) to quantify the decline in mitochondrial fluorescence, which clearly distinguished between the subpopulations of cells that did and did not undergo a loss of $\Delta\Psi$ over their lifespan (referred to as $\Delta\Psi-$ and $\Delta\Psi+$, respectively). The fraction of $\Delta\Psi-$ and $\Delta\Psi+$ cells was 30% ± 10% and 58% ± 10%, respectively (n = 77; Figure 3E). In the remaining 12% of cells, we were unable to clearly interpret the evolution of the preCox4-mCherry signal.

Analysis of the mean mitochondrial fluorescence at cell birth, SEP, and death indicated that the loss of $\Delta\Psi$ had already occurred in $\Delta\Psi-$ cells by the SEP (Figure 3F). Indeed, averaging all of the $\Delta\Psi-$ cell data to precisely time and order the events demonstrated that the decline in $\Delta\Psi$ began at 5.6 ± 1.3 hr after cell birth and reached baseline 10.1 ± 0.9 hr later (Figure 3G). Intriguingly, the SEP occurred only 3 ± 1.9 hr after $\Delta\Psi$ had reached zero, strongly suggesting a causal link between these two events. The timing of these events is compatible with the typical 15 hr decay in growth rate observed in ethidium-bromide-treated young cells (Veatch et al., 2009).

Overall, the behavior of $\Delta\Psi-$ cells appeared to be in good agreement, both qualitatively and quantitatively, with the findings of Veatch et al. However, we observed that the SEP occurred even in cells that did not display a decline in $\Delta\Psi$ (Figure 3D), arguing against a role for $\Delta\Psi$ in the transition to senescence. To further examine the differences between $\Delta\Psi+$ and $\Delta\Psi-$ cells, we measured the time from SEP to death and from birth to SEP in the two populations. The post-SEP survival time for $\Delta\Psi-$ cells was much longer than that of the $\Delta\Psi+$ cells (36.8 ± 4 hr versus 19.3 ± 3 hr, respectively; $p = 10^{-5}$; Figures 3H and S8), which suggested that the $\Delta\Psi-$ cells were in a

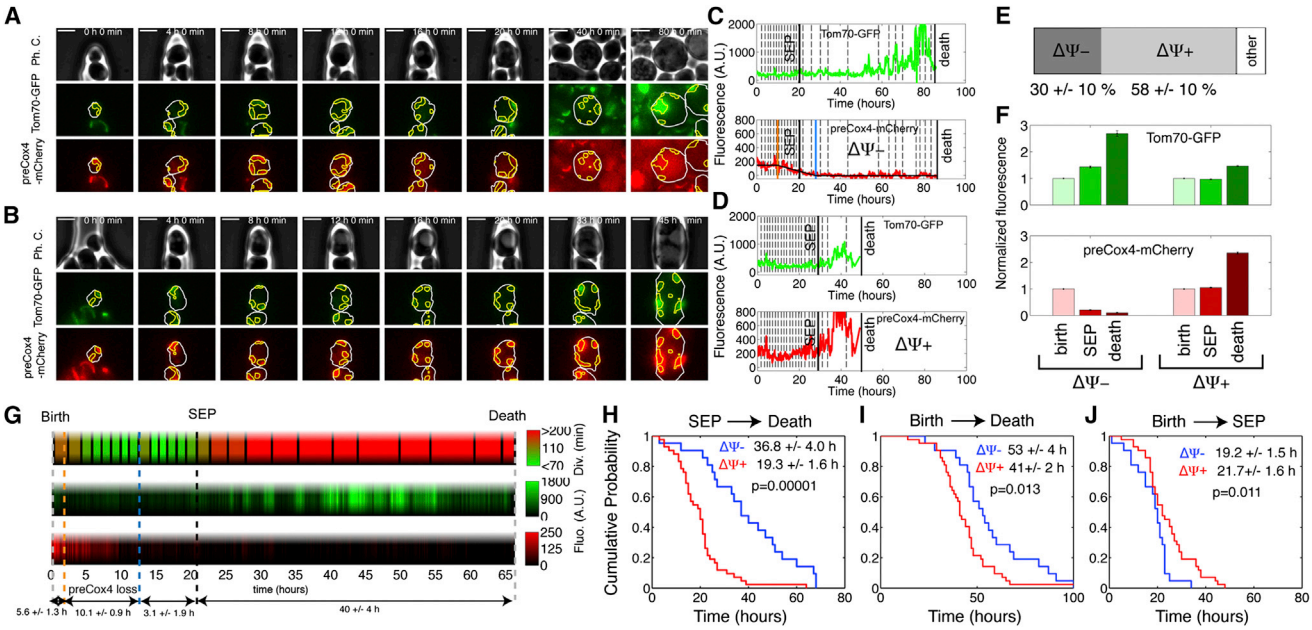

Figure 3. Decline in Mitochondrial Membrane Potential in Individual Mother Cells

(A and B) Time-lapse sequence of phase contrast and fluorescence (Tom70-GFP and preCox4-mCherry) images showing the successive divisions of individual cells with (A) and without (B) a decline in mitochondrial membrane potential. The white and yellow lines indicate the cell and mitochondrial contours, respectively. The scale bar represents 4 μm.

(C and D) Quantification of mitochondrial markers over time for the cells displayed in (A) and (B), respectively. Vertical dashed lines indicate budding events, and solid vertical lines indicate the SEP and cell death. The preCox4-mCherry signal was fitted to a piecewise model to quantify the change in mitochondrial membrane potential. Vertical orange and blue lines in (C) indicate the onset and end of fluorescence decay, respectively. ΔΨ− and ΔΨ+ indicate cells in which a decline in mitochondrial preCox4-mCherry fluorescence was or was not detected, respectively. a.u., arbitrary units.

(E) Fraction of aging mother cells with or without a decline in mitochondrial function (n = 77).

(F) Average level of Tom70-GFP and preCox4-mCherry fluorescence in a population of cells at cell birth, SEP, and death. Measurements are normalized to the levels at cell birth.

(G) Representative trajectory of an individual cell illustrating the typical order of events in the lifespan of ΔΨ− cells (top, cell-cycle duration; middle, Tom70-GFP level; bottom, preCox4-mCherry level). The average duration between the indicated events are shown at the bottom and are the mean ± SE of all ΔΨ− cells processed in this analysis (n = 23).

(H–J) Cumulative probability histograms of interval duration from SEP to death (H), birth to death (I), and birth to SEP (J). The numbers indicate the median time associated with the distribution for ΔΨ− (blue lines) and ΔΨ+ (red lines).

physiological state that conferred metabolic longevity, probably linked to the loss of respiration. In keeping with this, ΔΨ− cells also had longer overall lifespans than ΔΨ+ cells (53 ± 4 hr versus 41 ± 2 hr; p = 0.013; Figure 3I). Interestingly, there was no significant difference in the RLS of ΔΨ− and ΔΨ+ cells (p = 0.3; Figure S9), in agreement with previous findings (Kaeberlein and Kennedy, 2005; Heeren et al., 2009). The SEP occurred slightly yet significantly earlier in ΔΨ− cells than in ΔΨ+ cells (19.2 ± 1.5 hr versus 21.7 ± 1.6 hr after birth, respectively; p = 0.011; Figure 3J). Collectively, these data suggest that the shift to a slow replicative rate by ΔΨ− cells reflects a transition between two metabolic states rather than entry into senescence.

The Decline in ΔΨ Is Age-Independent

The hypothesis that ΔΨ is linked to the transition to senescence assumes that loss of ΔΨ is an age-dependent process. This derives from the observations that old (but not young) mothers generate a high proportion of *petite* daughters (Veatch et al., 2009) and that aging mothers show reduced mitochondrial membrane potential (Hughes and Gottschling, 2012). However, we noted that the time between the onset of loss of ΔΨ and the appearance of the slow-growth phenotype was on average larger than 13 hr (see Figure 3G). Thus, the physiological consequences of the decline in ΔΨ were not detected until long after its onset, which could have resulted in the interpretation that loss of ΔΨ occurs only in old mother cells. Therefore, we sought to determine whether the onset of loss of ΔΨ was age-dependent or occurred in a spontaneous and age-independent manner.

For this, we used a computational analysis to compare the experimental distribution of the time at which ΔΨ began to decline in the population of mother cells with two models in which the loss of ΔΨ is hypothesized to be age-independent or age-dependent. We assumed that the probability of cell death per generation for a cell of replicative age n, referred to as q(n), increased quadratically with n: $q(n) = q_0 \times n^2$ (where q_0 is a constant; Figure 4A), as proposed previously (Gillespie et al., 2004). Because the RLS of ΔΨ+ and ΔΨ− cells were identical (Figure S8), we used the same value of q_0 for both cell types. We implemented a stochastic simulation of a lifespan assay according to this set of rules in MATLAB (Supplemental Experimental

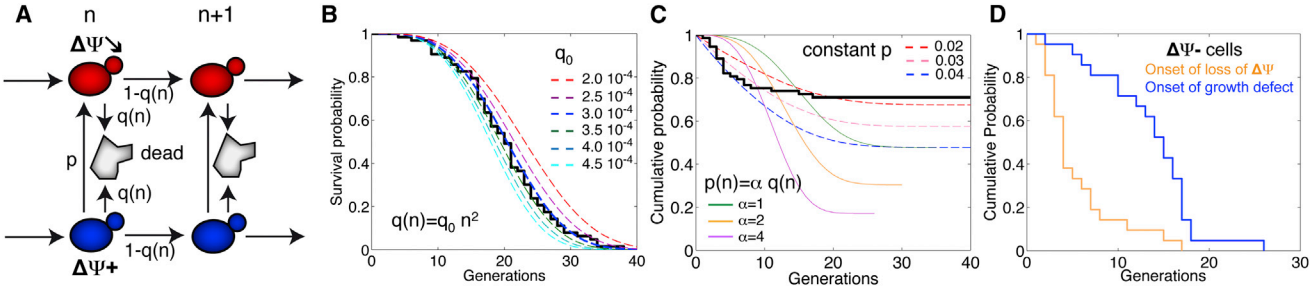

Figure 4. Age-Independent Decline in Mitochondrial Membrane Function in Aging Mother Cells

(A) Model for the transition from the ΔΨ+ state (blue cells) to a state in which ΔΨ starts declining (red cells) in cells of replicative age n. The probability of dying (gray cells) at each generation n is set by q(n). We define p as the probability of undergoing the transition to the onset of loss of ΔΨ.

(B) Numerical simulation of the RLS of mother cells, assuming a quadratic increase of q with n: $q = q_0 n^2$. Each dashed colored line corresponds to the value of q_0 as shown. The black line represents the experimentally obtained data.

(C) Cumulative probability of loss of ΔΨ from numerical simulations corresponding to the model described in (A) (colored lines) compared with the experimentally determined timing of the onset of ΔΨ decline (solid black line). Dashed colored lines correspond to the indicated p values (assuming p is constant), and the solid colored lines correspond to a model in which p is age-dependent (i.e., p is proportional to q).

(D) Experimental cumulative probability of onset of ΔΨ decline (orange line) and onset of the growth defect (blue line).

Procedures) and found that the quadratic model for cell mortality fitted the experimental RLS curve very accurately, yielding a best fit for q_0 of 3×10^{-4} (Figure 4B).

For the age-independent model, we assumed that the onset of loss of ΔΨ occurred randomly according to a constant probability per generation p. Using values of p from 0.02 to 0.04, we obtained a reasonable agreement between the simulation and the cumulative probability of maintaining high ΔΨ as a function of age (Figure 4C, dashed lines). The experimental distribution was obtained by measuring the timing of the onset of loss of ΔΨ using the fitting procedure described in Figure 3C. In particular, it is striking that this model could semiquantitatively explain both the timescale associated with the loss of ΔΨ (experimentally determined to be 5.6 ± 1.3 hr, corresponding to approximately four generations; in the simulation, ~50% of the cells that ultimately became ΔΨ− have done so after six generations) and the fraction of ΔΨ− cells in the population of aging mothers (experimentally determined to be 30% ± 10%; in the simulation, ~40% using p = 0.03) using a single free parameter.

For the age-dependent model, we assumed that the probability p of switching to a state in which ΔΨ declines was proportional to q(n): $p(n) = \alpha\, q(n)$, where α is a constant. This model appeared to be incompatible with the observations, regardless of the value of α: indeed, the model could not accommodate either the short timescale decay of the experimental data or the high fraction of ΔΨ+ cells that remained in the population at the end of the lifespan (Figure 4C, solid lines).

The finding that the onset of loss of ΔΨ appeared to follow Poisson statistics was not inconsistent with the late occurrence of *petite* daughters observed in old mothers (Veatch et al., 2009). Indeed, because the decline of ΔΨ occurs over ~10 hr (Figure 3G), the growth defect (used to assess *petite*ness) appeared long after the onset of the decline in ΔΨ (Figure 4D).

This quantitative analysis therefore suggested that the ΔΨ− phenotype appears stochastically in the population of aging mothers, with a constant age-independent probability $p \sim 0.03$ per generation. To probe this further, we compared this p value with the probability of spontaneous formation of *petite* colonies in bulk cultures. We performed standard plating assays to measure the fraction R of *petite* colonies in the same strain as used in the microfluidics assay. The probability of *petite* formation can be deduced from R and the specific growth rates of wild-type and *petite* cells (see the Supplemental Information), which we measured using standard turbidity measurements. The fraction R measured (33.5% ± 1%; Table S1) gave p = 0.051 ± 0.001, which is clearly in the same range as the value obtained in the microfluidics lifespan assay. We conclude that the loss of ΔΨ in a fraction of aging mothers is very likely to originate from the spontaneous loss or mutation of mtDNA and is therefore not a hallmark of aging.

The Decline in ΔΨ Is Incompatible with Daughter Cell Rejuvenation

An essential feature of yeast aging is the ability of daughters of aged mothers to recover a full lifespan potential, that is, to undergo rejuvenation. This striking property was first characterized by measuring the mean generation time of daughters born from mothers of varying ages (Egilmez and Jazwinski, 1989). We investigated the inheritance of the ΔΨ− phenotype in daughters of aging mothers and directly monitored the rejuvenation process using the CLiC device, which allowed us to track the fate of daughters in the trapping area over approximately two to three generations.

Importantly, we found that the decline in preCox4-mCherry fluorescence in ΔΨ− mothers was transmitted to their successive buds (Figures 5A and 5B), suggesting that the loss of respiration was fully inherited by the daughters. We also measured the cell cycle duration of the individual progeny and found that the entire progeny of slowly dividing ΔΨ− mother cells displayed a slow-growth phenotype (monitored over >40 hr; Figure 5C; Movie S4). This observation is reminiscent of the "clonal senescence" described earlier in yeast (Lai et al., 2002). In striking contrast, daughters of post-SEP ΔΨ+ mothers eventually gave rise to progeny with rapid cell division, indicating that rejuvenation of this lineage occurred even after the SEP (Figure 5D; Movie S5).

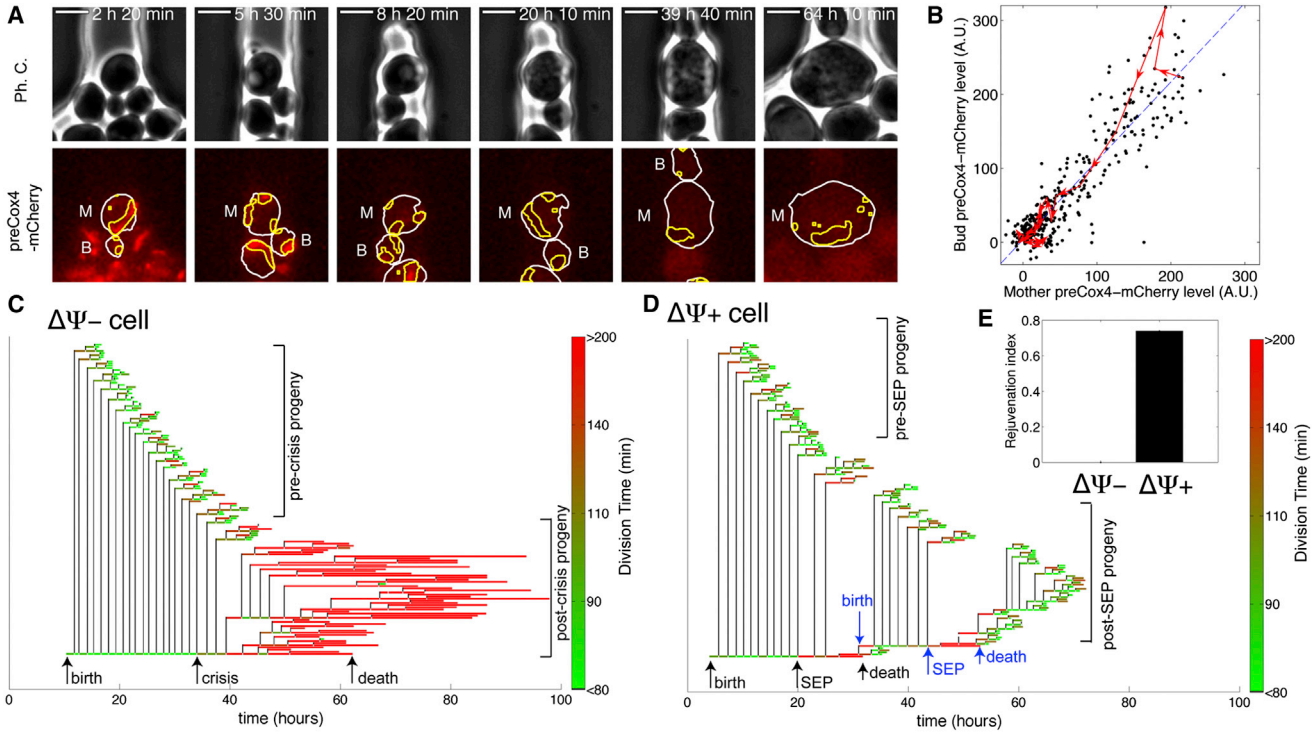

Figure 5. Inheritance of Mitochondrial Markers and Daughter Cell Rejuvenation

(A) Time-lapse sequence of phase contrast and fluorescence images showing the decay of the mitochondrial preCox4-mCherry signal in mother (M) and its successive bud (B). The white and yellow lines indicate the cell and mitochondrial contours, respectively. The scale bar represents 4 μm.

(B) preCox4-mCherry signals in bud versus mother upon cell division. The scatter plot (black dots) pools all the data obtained from ΔΨ− cells (n = 365 division events). The red line shows the decrease in preCox4-mCherry fluorescence for one specific mother cell. The blue dashed line is a fit to the scatter plot (B = 1.06 [±0.05] M + 3.6 [± 4]), showing equal distribution of fluorescence between the mother and bud.

(C and D) Sample pedigrees of single ΔΨ− (C) and ΔΨ+ (D) cells, showing the successive divisions of its progeny. Color coding represents the division time.

(E) Rejuvenation index based on the behavior of daughters of post-SEP ΔΨ+ and ΔΨ− mother cells.

We defined a rejuvenation index as the fraction of post-SEP ΔΨ+ or postcrisis ΔΨ− mothers that generated a progeny with normal cell-cycle durations. Using this definition, the rejuvenation index of ΔΨ− and ΔΨ+ cells was measured to be 0 and 0.74, respectively (n = 77; Figure 5E). This quantification thus confirmed that the loss of ΔΨ led to an irreversible phenotype that was inconsistent with daughter cell rejuvenation. Therefore, these results further suggested that ΔΨ loss should not be regarded as part of the mechanism leading to the entry into cellular senescence, as proposed earlier (Veatch et al., 2009; Hughes and Gottschling, 2012).

Interestingly, our analysis revealed that scoring the clonal replicative slowdown of the progeny of an aging mother was a reliable method of determining whether this cell had transitioned to the ΔΨ− state, regardless of preCox4-mCherry marker measurements. We used this tight correlation to assess the fraction of ΔΨ− cells in other strain backgrounds. S288C-related strains have been shown to display a very high (yet variable) level of *petite* cells compared with W303 or natural strains (Dimitrov et al., 2009). Indeed, in replicative aging assays, we found that only 9% of W303 cells were ΔΨ− cells, which is much lower than in a S288C background and in good agreement with plating assays (Table S1). Thus, the large fraction of cells that undergo a transition to a ΔΨ− phenotype during their lifespan is somewhat specific to the S288C background.

Budding Is Accompanied by Dynamic Mitochondrial Fusion in Aging Mothers

Our finding that the loss of ΔΨ is age-independent does not preclude the involvement of mitochondrial dysfunction in the aging process. Indeed, it has been proposed that asymmetrical segregation of damaged mitochondria could be a mechanism for the rejuvenation of daughter cells (Seo et al., 2010; McFaline-Figueroa et al., 2011). During our mitochondrial marker experiments, we noted that Tom70-GFP fluorescence was dramatically increased in post-SEP mothers (Figure 3); therefore, we asked whether this high fluorescence level was transmitted to the progeny. Whereas the fluorescence level was identical in pre-SEP mothers and their buds, it remained much higher in post-SEP mothers than in their buds (Figure 6A). This phenomenon was observed in both ΔΨ− and ΔΨ+ cells, demonstrating that it was independent of ΔΨ.

Analysis of single-cell images revealed that small-budded cells contained very bright clusters of mitochondria that disappeared upon cell division (Figure 6B; Movie S6). Indeed, quantification of the mean mitochondrial Tom70-GFP signal revealed

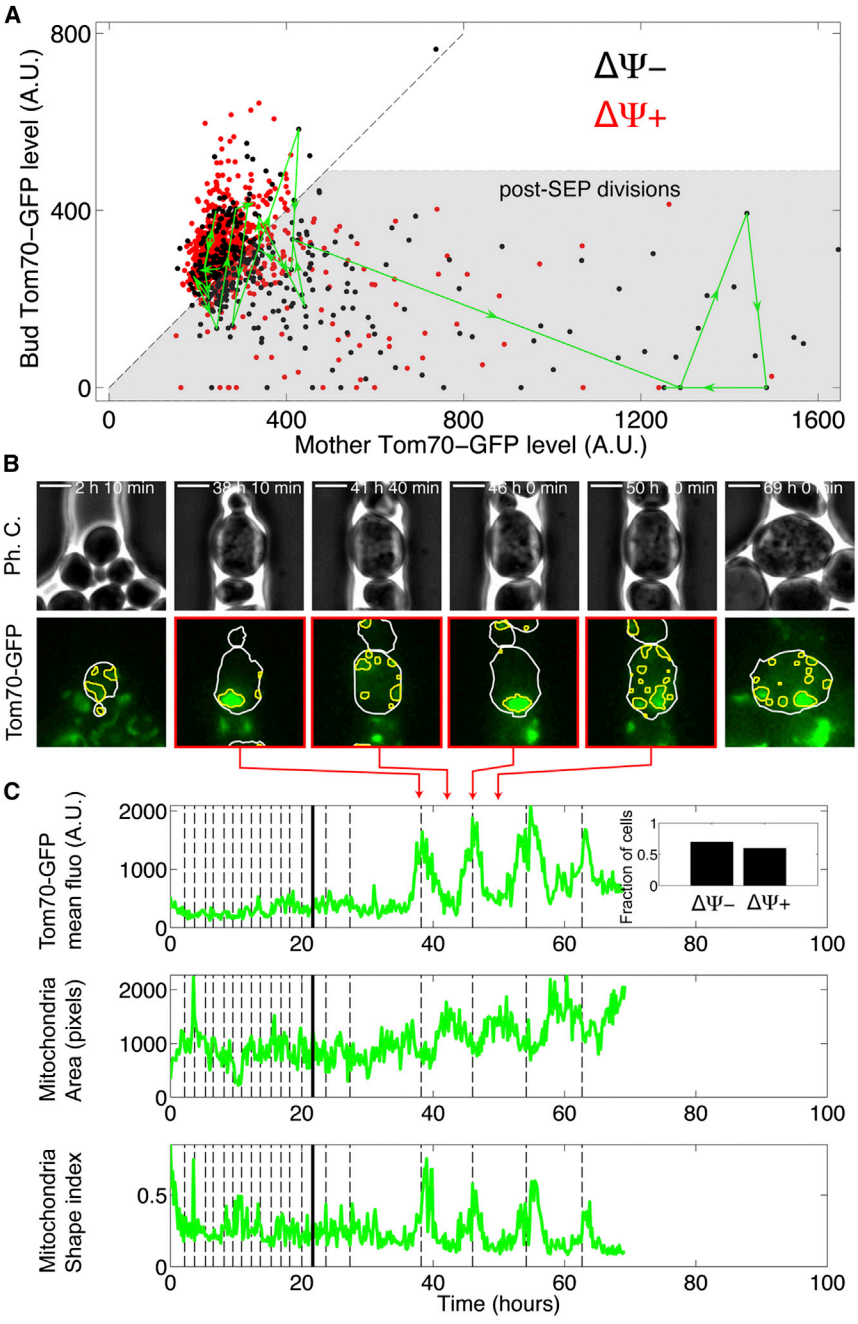

Figure 6. Inheritance of Mitochondrial Markers and Rejuvenation in ΔΨ− and ΔΨ+ Cells

(A) Mitochondrial Tom70-GFP signal in bud versus mother upon cell division. The scatter plots pool all the data obtained from ΔΨ− (black) and ΔΨ+ (red) cells. The green line shows the signal trajectory for a specific cell. The dashed line indicates the diagonal, and the shaded area roughly indicates the data corresponding to post-SEP mother cells.

(B) Time-lapse sequence of phase contrast and Tom70-GFP fluorescence images at the indicated times, highlighting the oscillations in the mitochondrial Tom70-GFP level in a post-SEP mother cell. The scale bar represents 4 μm.

(C) Quantification of mitochondrial Tom70-GFP level, mitochondrial area, and the overall shape index (defined as the area divided by the square of the perimeter) for the cell displayed in (B). Inset shows the fraction of cells displaying oscillatory behavior in mitochondrial fusion/fission.

that this phenomenon occurred in phase with the cell cycle (Figure 6C) and was in part due to the decrease in total mitochondrial area and overall rounding of its shape. We found that ~60% of cells exhibited this unexpected cycling behavior of mitochondria fusion/fission after the SEP. These results thus revealed an unexpected feature of mitochondrial dynamics triggered by the SEP. We speculate that the transient formation of mitochondrial clusters upon budding might impair their transmission and thus protect the daughter cells from importing damaged mitochondria, as previously described (McFaline-Figueroa et al., 2011).

DISCUSSION

Quantitative Real-Time Imaging of Single Yeast Cells Reveals an Unexpectedly Abrupt Entry into Senescence

In this study, we described a microfluidic device that allowed us to quantitatively assess both the transition to senescence and the decline in ΔΨ in individual yeast cells. The device design allowed us to start our assays with unstressed virgin cells and to monitor cellular processes with an unmatched temporal resolution (Lee et al., 2012; Xie et al., 2012; Zhang et al., 2012). Using this methodology, we discovered that aging yeast cells undergo a sharp transition from fast to slow growth that occurs within three division cycles. It seems likely that this remarkably abrupt entry into senescence could not be detected in experiments in which single-cell data were pooled (Egilmez and Jazwinski, 1989) or in which variability in cell fate was not fully taken into account (Lee et al., 2012; Xie et al., 2012; Zhang et al., 2012). Indeed, we confirmed that pooling of the data masks the distinct replicative characteristics of pre-SEP and post-SEP cells, thus artificially smoothing the transition to senescence.

Our quantitative analysis of pre- and post-SEP cell division sheds light on the replicative senescence state. First, we found that post-SEP cells exhibit a loss of cell-cycle control, as illustrated by the large increase in CV of cell-cycle duration following the SEP. This is a clear hallmark of senescence, although further studies will be necessary to identify the molecular mechanisms leading to the loss of cell-cycle control and ultimately to division

arrest (Delaney et al., 2013). Second, the apparent switch-like transition in cellular physiology challenges the widely accepted idea that cellular aging is a gradual process. However, a sharp SEP does not preclude the involvement of progressively accumulated damaged cellular components, as proposed long ago (Egilmez and Jazwinski, 1989). Indeed, it is possible that the SEP is triggered once deleterious factors reach a critical level; if so, the sharp entry into a slow replicative mode would actually highlight the remarkable buffering capabilities of the cell-cycle machinery against cellular damage.

Loss of $\Delta\Psi$ Is Age-Independent and Is Incompatible with Daughter Cell Rejuvenation

The possible role of age-dependent mitochondrial dysfunction in the transition to replicative senescence was observed in a study of aging mother cells that gave rise to slow-growing *petite* daughters (Veatch et al., 2009) and was supported by further work showing direct evidence for the loss of $\Delta\Psi$ in aging mothers (Hughes and Gottschling, 2012). Consistent with these findings, we identified a fraction of cells (~30%) that showed a progressive loss in $\Delta\Psi$ during the transition to senescence. However, the vast majority of cells maintained normal $\Delta\Psi$ throughout their lifespan and both $\Delta\Psi-$ and $\Delta\Psi+$ cells apparently passed through the SEP. Further statistical analysis of the onset of loss of $\Delta\Psi$ in aging mothers supported a model in which the transition to a nonrespiring state was a spontaneous and age-independent event and was incompatible with an age-dependent model, as assumed by Veatch et al. This result was reinforced by the fact that the probability per generation of randomly transitioning to a nonrespiring state, as deduced from our single-cell experiments, was comparable to the probability measured from *petite* formation assays in bulk.

Our quantitation of mother-daughter inheritance of the $\Delta\Psi-$ phenotype in individual cells allowed us to establish a direct link between the observed loss of $\Delta\Psi$ in aging mothers (Hughes and Gottschling, 2012) and the high frequency of the *petite* phenotype in daughters of old mothers (Veatch et al., 2009). We found that the decline in $\Delta\Psi$ was both irreversible and heritable and resulted in a clonal lengthening of the cell cycle in the entire progeny of individual $\Delta\Psi-$ mothers (Lai et al., 2002). This phenomenon could be interpreted as the mother cells reaching a point of no return, beyond which rejuvenation is impaired. However, this view is challenged by corresponding measurements showing that the vast majority of aging $\Delta\Psi+$ mothers give birth to a rejuvenated lineage, even after they have passed the SEP. Interestingly, this latter observation suggests that the putative asymmetrical segregation of deleterious factors is not completely abolished in post-SEP mothers. Therefore, whereas the SEP is an irreversible hallmark of aging for mother cells, further investigation will be necessary to decipher the rules that limit the recovery of replicative potential in daughters of very old mothers.

Two factors in particular may explain the divergent conclusions of our study and that of Veatch et al. (2009) regarding the association between loss of $\Delta\Psi$ and senescence. One is the large variability in the incidence of the *petite* phenotype across the different yeast strains. Other studies in the same laboratory reported proportions of nonrespiring cells ranging from ~30% (Lindstrom et al., 2011) to ~95% (Veatch et al., 2009; Hughes and Gottschling, 2012) in the S288C background, which was proposed to originate from variations in genes controlling the maintenance of mtDNA (Dimitrov et al., 2009; Hess et al., 2009; Lindstrom et al., 2011). We confirmed that the S288C background has an unusually high (and variable, see Table S2) incidence of *petite* cells compared with other lab (W303) or natural (RM11) strain backgrounds (Dimitrov et al., 2009; Hess et al., 2009). This suggests that the association between loss of $\Delta\Psi$ and replicative aging proposed by Veatch et al. may be tied to the unusually high *petite* formation rate in the strain used.

Interestingly, two recent studies showed an unexplained bimodality in the morphology and expression of stress markers of aging mother cells in microfluidics-based RLS assays using S288C strains (Lee et al., 2012; Xie et al., 2012). We hypothesize that this observation could reflect a heterogeneous mixture of respiring and nonrespiring cells. In addition, even though both cell types display the same lifespan in a wild-type strain (Kaeberlein and Kennedy, 2005; Heeren et al., 2009), one should pay attention to how much of the extension of lifespan observed in some longevity mutants is due to the presence of *petite* cells when using the widely studied S288C background (i.e., potentially misleading genetic interactions).

Second, our results highlight the fact that an age-independent event (i.e., that follows Poisson statistics) may be perceived as age-dependent if the time between the event and readout is protracted. For instance, statistical analysis of cell-cycle duration revealed that the growth defect occurs only in old mothers and thus appears to be age-dependent, but the putative triggering event—the onset of the decline in $\Delta\Psi$—occurs at a constant rate per generation (Figure 4D). This nonintuitive and misleading kinetic effect presumably underlies the assumption that the occurrence of *petite* daughters is age-dependent in Veatch et al. (2009).

Interestingly, this argument has unexpected implications for deciphering the causality of events during the transition to senescence. In theory, one cannot exclude that cellular aging originates from spontaneously arising events, the frequency of which is not enhanced by cellular age, but which initiate a temporally controlled cascade of events leading to cell death. The large cell-to-cell variability in the lifespan (CV = 0.45; data not shown) is likely to reflect the role played by these stochastic processes in the control of longevity (Elowitz et al., 2002; Gandhi et al., 2011).

The Relationship between Mitochondrial Function, Senescence, and Daughter Cell Rejuvenation

Although our results argue against a role for loss of $\Delta\Psi$ in the entry into senescence, they do not contradict the link between loss of $\Delta\Psi$ and increased loss of heterozygosity (LOH) (Veatch et al., 2009). LOH has been reported to occur through a different mechanism in respiring aging cells (Lindstrom et al., 2011), which, in the light of our results, appears to confirm that increased genomic instability is a hallmark of aging in yeast (McMurray and Gottschling, 2003), independently of the respiration status.

Recently, Hughes and Gottschling (2012) found that overexpression of genes that promote vacuolar acidity delayed the

onset of loss of $\Delta\Psi$ and extended longevity. Because these genes were known regulators of mitochondrial function (Dimmer et al., 2002), it is likely that their overexpression in a strain with a high frequency of nonrespiring cells may have reduced the rate of *petite* formation, a scenario that is compatible with our model.

Our study reveals insights into mitochondrial dynamics in aging cells. We found that mitochondrial markers increased significantly in post-SEP cells and that large mitochondrial clusters (Scheckhuber et al., 2007) present in post-SEP small-budded cells disappeared at cell division. As a consequence, daughters of post-SEP mother cells inherited fewer mitochondria. Mitochondrial clustering was manifest in both respiring and nonrespiring post-SEP cells, suggesting that the event is unrelated to the loss of $\Delta\Psi$ (Seo et al., 2010). Notably, the mitochondrial clusters were not observed in pre-SEP mothers, indicating that it is a consequence rather than a cause of the transition to senescence. We speculate that the transient formation of mitochondrial clusters upon budding might impair their transmission and thus protect the daughter cells from importing damaged mitochondria, as previously described (McFaline-Figueroa et al., 2011, Dalton and Carroll, 2013).

CONCLUSION

Our study introduces a microscopy-based methodology to track the fate of single yeast cells from birth to death. Our results emphasize the unique ability of single-cell analysis to monitor and decipher the complex biological processes associated with replicative aging. We characterized in detail the dynamics of the transition to cellular senescence and challenged a well-established model in which the loss of membrane potential appeared to be a key aspect of the transition to senescence. Our analysis also raises several fundamental questions: what are the mechanisms leading to cell-cycle slowdown and the SEP? How is the scenario proposed here influenced by specific longevity mutations? Further work combining our methodology with classical genetic studies will undoubtedly help to answer these questions.

EXPERIMENTAL PROCEDURES

Strains and Plasmids

All strains used in this study are congenic to S288C, unless specified. Additional details can be found in the Supplemental Experimental Procedures.

Microfluidics

The microfluidic master was made using standard soft lithography techniques with SU-8 photoresist and custom polymer masks (Selba). Microchannels were cast by curing polydimethylsiloxane (PDMS) (Sylgard 184) and covalently binding the PDMS to a coverslip with a plasma cleaner (Diener). See the Supplemental Experimental Procedures for the detailed protocol.

Time-Lapse Microscopy

Cells were grown overnight, transferred to fresh medium the next morning, and allowed to grow to log phase until transfer to the microfluidic device in the afternoon. During the experiments, synthetic complete medium with 2% glucose (SCD) was continuously perfused through the device using a peristaltic pump (Ismatec; flow rate: 25 μl/min). Images were acquired every 10 min using a wide-field motorized epifluorescence microscope. See the Supplemental Experimental Procedures for the detailed protocol.

Image Analysis

Raw images were processed using custom software, termed phyloCell, using MATLAB and the image-processing toolbox. This software is freely available upon request. See the Supplemental Experimental Procedures for a detailed description of the image processing and quantification pipeline.

Petite Colony-Plating Assay

Cells were grown overnight in liquid YPD media and the next morning were plated on yeast extract peptone ethanol containing 2% glycerol and 0.1% glucose to monitor the formation of *petite* colonies, according to standard techniques. After 2 days of growth, the fraction of *petites* was scored by counting 200 cells from a triplicate experiment. The probability of *petite* formation per generation was calculated as described in the Supplemental Experimental Procedures.

Mathematical Model for *Petite* Formation in Aging Cells

See the Supplemental Experimental Procedures for the detailed model used to fit the experimental distribution of *petite* emergence in aging cells.

Replicative Aging Assay with Microdissection

RLS assays were performed on plates as previously described (Kennedy et al., 1994), using a solid synthetic medium to match the conditions used in the microfluidics experiments.

SUPPLEMENTAL INFORMATION

Supplemental Information includes Supplemental Experimental Procedures, nine figures, two tables, and six movies and can be found with this article online at http://dx.doi.org/10.1016/j.celrep.2013.11.013.

ACKNOWLEDGMENTS

We are very grateful to Dan Gottschling for providing mitochondrial markers used throughout this study. We acknowledge fruitful discussions regarding microfabrication with André Estevez-Torres, Christian Rick, and Hicham Majjad. We are grateful to Daniel Riveline for giving us the opportunity to use the Institut de Sciences et d'Ingénierie Supramoléculaire cleanroom. We also thank David Stillmann and Joseph Schacherer for providing yeast strains and Bertrand Séraphin for sharing his tetrad dissection microscope. We thank Zhou Xu, Teresa Teixeira, Michael Knop, Michel Toledano, and Poonam Bheda for insightful discussion and for a critical reading of the manuscript. We thank Marc Koch for imaging the microfabricated master wafer. This work was supported by the French Agence Nationale Pour la Recherche (ANR PCVI-2008-003) and the ATIP-AVENIR program.

Received: July 18, 2013
Revised: October 23, 2013
Accepted: November 7, 2013
Published: December 12, 2013

REFERENCES

Afonso, B., Silver, P.A., and Ajo-Franklin, C.M. (2010). A synthetic circuit for selectively arresting daughter cells to create aging populations. Nucleic Acids Res. *38*, 2727–2735.

Aguilaniu, H., Gustafsson, L., Rigoulet, M., and Nyström, T. (2003). Asymmetric inheritance of oxidatively damaged proteins during cytokinesis. Science *299*, 1751–1753.

Bitterman, K.J., Medvedik, O., and Sinclair, D.A. (2003). Longevity regulation in *Saccharomyces cerevisiae*: linking metabolism, genome stability, and heterochromatin. Microbiol. Mol. Biol. Rev. *67*, 376–399.

Charvin, G., Cross, F.R., and Siggia, E.D. (2008). A microfluidic device for temporally controlled gene expression and long-term fluorescent imaging in unperturbed dividing yeast cells. PLoS ONE *3*, e1468.

Dalton, C.M., and Carroll, J. (2013). Biased inheritance of mitochondria during asymmetric cell division in the mouse oocyte. J. Cell Sci. *126*, 2955–2964.

Delaney, J.R., Chou, A., Olsen, B., Carr, D., Murakami, C., Ahmed, U., Sim, S., An, E.H., Castanza, A.S., Fletcher, M., et al. (2013). End-of-life cell cycle arrest contributes to stochasticity of yeast replicative aging. FEMS Yeast Res. *13*, 267–276.

Dimitrov, L.N., Brem, R.B., Kruglyak, L., and Gottschling, D.E. (2009). Polymorphisms in multiple genes contribute to the spontaneous mitochondrial genome instability of *Saccharomyces cerevisiae* S288C strains. Genetics *183*, 365–383.

Dimmer, K.S., Fritz, S., Fuchs, F., Messerschmitt, M., Weinbach, N., Neupert, W., and Westermann, B. (2002). Genetic basis of mitochondrial function and morphology in *Saccharomyces cerevisiae*. Mol. Biol. Cell *13*, 847–853.

Egilmez, N.K., and Jazwinski, S.M. (1989). Evidence for the involvement of a cytoplasmic factor in the aging of the yeast *Saccharomyces cerevisiae*. J. Bacteriol. *171*, 37–42.

Elowitz, M.B., Levine, A.J., Siggia, E.D., and Swain, P.S. (2002). Stochastic gene expression in a single cell. Science *297*, 1183–1186.

Erjavec, N., Larsson, L., Grantham, J., and Nyström, T. (2007). Accelerated aging and failure to segregate damaged proteins in Sir2 mutants can be suppressed by overproducing the protein aggregation-remodeling factor Hsp104p. Genes Dev. *21*, 2410–2421.

Gandhi, S.J., Zenklusen, D., Lionnet, T., and Singer, R.H. (2011). Transcription of functionally related constitutive genes is not coordinated. Nat. Struct. Mol. Biol. *18*, 27–34.

Gehlen, L.R., Nagai, S., Shimada, K., Meister, P., Taddei, A., and Gasser, S.M. (2011). Nuclear geometry and rapid mitosis ensure asymmetric episome segregation in yeast. Curr. Biol. *21*, 25–33.

Gillespie, C.S., Proctor, C.J., Boys, R.J., Shanley, D.P., Wilkinson, D.J., and Kirkwood, T.B.L. (2004). A mathematical model of ageing in yeast. J. Theor. Biol. *229*, 189–196.

Guarente, L. (2008). Mitochondria—a nexus for aging, calorie restriction, and sirtuins? Cell *132*, 171–176.

Heeren, G., Rinnerthaler, M., Laun, P., von Seyerl, P., Kössler, S., Klinger, H., Hager, M., Bogengruber, E., Jarolim, S., Simon-Nobbe, B., et al. (2009). The mitochondrial ribosomal protein of the large subunit, Afo1p, determines cellular longevity through mitochondrial back-signaling via TOR1. Aging (Albany, N.Y. Online) *1*, 622–636.

Hess, D.C., Myers, C.L., Huttenhower, C., Hibbs, M.A., Hayes, A.P., Paw, J., Clore, J.J., Mendoza, R.M., Luis, B.S., Nislow, C., et al. (2009). Computationally driven, quantitative experiments discover genes required for mitochondrial biogenesis. PLoS Genet. *5*, e1000407.

Houtkooper, R.H., Mouchiroud, L., Ryu, D., Moullan, N., Katsyuba, E., Knott, G., Williams, R.W., and Auwerx, J. (2013). Mitonuclear protein imbalance as a conserved longevity mechanism. Nature *497*, 451–457.

Hughes, A.L., and Gottschling, D.E. (2012). An early age increase in vacuolar pH limits mitochondrial function and lifespan in yeast. Nature *492*, 261–265.

Kaeberlein, M., and Kennedy, B.K. (2005). Large-scale identification in yeast of conserved ageing genes. Mech. Ageing Dev. *126*, 17–21.

Kennedy, B.K., Austriaco, N.R., Jr., and Guarente, L. (1994). Daughter cells of *Saccharomyces cerevisiae* from old mothers display a reduced life span. J. Cell Biol. *127*, 1985–1993.

Khmelinskii, A., Meurer, M., Knop, M., and Schiebel, E. (2011). Artificial tethering to nuclear pores promotes partitioning of extrachromosomal DNA during yeast asymmetric cell division. Curr. Biol. *21*, R17–R18.

Lai, C.-Y., Jaruga, E., Borghouts, C., and Jazwinski, S.M. (2002). A mutation in the ATP2 gene abrogates the age asymmetry between mother and daughter cells of the yeast *Saccharomyces cerevisiae*. Genetics *162*, 73–87.

Lee, S.S., Avalos Vizcarra, I., Huberts, D.H.E.W., Lee, L.P., and Heinemann, M. (2012). Whole lifespan microscopic observation of budding yeast aging through a microfluidic dissection platform. Proc. Natl. Acad. Sci. USA *109*, 4916–4920.

Lindstrom, D.L., and Gottschling, D.E. (2009). The mother enrichment program: a genetic system for facile replicative life span analysis in Saccharomyces cerevisiae. Genetics *183*, 413–422.

Lindstrom, D.L., Leverich, C.K., Henderson, K.A., and Gottschling, D.E. (2011). Replicative age induces mitotic recombination in the ribosomal RNA gene cluster of *Saccharomyces cerevisiae*. PLoS Genet. *7*, e1002015.

Liu, B., Larsson, L., Caballero, A., Hao, X., Oling, D., Grantham, J., and Nyström, T. (2010). The polarisome is required for segregation and retrograde transport of protein aggregates. Cell *140*, 257–267.

McFaline-Figueroa, J.R., Vevea, J., Swayne, T.C., Zhou, C., Liu, C., Leung, G., Boldogh, I.R., and Pon, L.A. (2011). Mitochondrial quality control during inheritance is associated with lifespan and mother-daughter age asymmetry in budding yeast. Aging Cell *10*, 885–895.

McMurray, M.A., and Gottschling, D.E. (2003). An age-induced switch to a hyper-recombinational state. Science *301*, 1908–1911.

Mortimer, R.K., and Johnston, J.R. (1959). Life span of individual yeast cells. Nature *183*, 1751–1752.

Scheckhuber, C.Q., Erjavec, N., Tinazli, A., Hamann, A., Nyström, T., and Osiewacz, H.D. (2007). Reducing mitochondrial fission results in increased life span and fitness of two fungal ageing models. Nat. Cell Biol. *9*, 99–105.

Seo, A.Y., Joseph, A.M., Dutta, D., Hwang, J.C., Aris, J.P., and Leeuwenburgh, C. (2010). New insights into the role of mitochondria in aging: mitochondrial dynamics and more. J. Cell Sci. *123*, 2533–2542.

Shcheprova, Z., Baldi, S., Frei, S.B., Gonnet, G., and Barral, Y. (2008). A mechanism for asymmetric segregation of age during yeast budding. Nature *454*, 728–734.

Sinclair, D.A., and Guarente, L. (1997). Extrachromosomal rDNA circles—a cause of aging in yeast. Cell *91*, 1033–1042.

Spokoini, R., Moldavski, O., Nahmias, Y., England, J.L., Schuldiner, M., and Kaganovich, D. (2012). Confinement to organelle-associated inclusion structures mediates asymmetric inheritance of aggregated protein in budding yeast. Cell Rep *2*, 738–747.

Unal, E., Kinde, B., and Amon, A. (2011). Gametogenesis eliminates age-induced cellular damage and resets life span in yeast. Science *332*, 1554–1557.

Veatch, J.R., McMurray, M.A., Nelson, Z.W., and Gottschling, D.E. (2009). Mitochondrial dysfunction leads to nuclear genome instability via an iron-sulfur cluster defect. Cell *137*, 1247–1258.

Wallace, D.C. (2005). A mitochondrial paradigm of metabolic and degenerative diseases, aging, and cancer: a dawn for evolutionary medicine. Annu. Rev. Genet. *39*, 359–407.

Wang, P., Robert, L., Pelletier, J., Dang, W.L., Taddei, F., Wright, A., and Jun, S. (2010). Robust growth of *Escherichia coli*. Curr. Biol. *20*, 1099–1103.

Xie, Z., Zhang, Y., Zou, K., Brandman, O., Luo, C., Ouyang, Q., and Li, H. (2012). Molecular phenotyping of aging in single yeast cells using a novel microfluidic device. Aging Cell *11*, 599–606.

Zhang, Y., Luo, C., Zou, K., Xie, Z., Brandman, O., Ouyang, Q., and Li, H. (2012). Single cell analysis of yeast replicative aging using a new generation of microfluidic device. PLoS ONE *7*, e48275.

Zhou, C., Slaughter, B.D., Unruh, J.R., Eldakak, A., Rubinstein, B., and Li, R. (2011). Motility and segregation of Hsp104-associated protein aggregates in budding yeast. Cell *147*, 1186–1196.